IEEE Access
Multidisciplinary | Rapid Review | Open Access Journal

Received September 29, 2019, accepted October 30, 2019, date of publication November 4, 2019,
date of current version November 15, 2019.

Digital Object Identifier 10.1109/ACCESS.2019.2951136

How Can Artificial Intelligence Help With Space Missions - A Case Study: Computational Intelligence-Assisted Design of Space Tether for Payload Orbital Transfer Under Uncertainties

XIANLIN REN[1,2], (Member, IEEE), AND YI CHEN[3], (Senior Member, IEEE)
[1]School of Mechatronics Engineering, University of Electronic Science and Technology of China, Chengdu 611731, China
[2]Institute of Electronic and Information Engineering of UESTC in Guangdong, Dongguan 523808, China
[3]School of Engineering, Newcastle University, Newcastle upon Tyne, NE1 7RU, U.K.

Corresponding authors: Xianlin Ren (renxianlin0@163.com) and Yi Chen (leo.chen@ieee.org)

This work was supported in part by the National Natural Science Foundation of China under Grant 51875090, and in part by the Natural Science Foundation of Guangdong Province under Grant 2018A030313320.

ABSTRACT In the era of artificial intelligence (AI), many industry sectors, including space exploration, have experienced a shift in the way business is conducted due to the widespread use of AI technologies. In the past few years, AI has become a key tool used to explore the universe in space missions. In this paper, a multi-objective optimal design for payload orbital transfer involving space tethers is proposed based on a computational intelligence-assisted design framework with the artificial wolf pack algorithm (AWPA). Enlightened by the social behaviors of a wolf pack and its swarm intelligence, the AWPA is utilized for optimization problems in which a logsig function randomly obtains assignments for parents and offspring. *Swarmwolf*, a simulation toolbox with given initial conditions. The proposed method effectively performs optimization tasks based on index of evolutionary pathway trends, has been defined to demonstrate the optimizing process. The results show that the proposed approach works expeditiously for the optimization of space tether model and its application.

INDEX TERMS Artificial intelligence, artificial wolf-pack algorithm, computational intelligence assisted design, evolutionary pathway, multi-objective optimization, payload orbital transfer, space tether.

I. INTRODUCTION

Reflecting one of the most innovative activities, artificial intelligence (AI) has become essential to the global economy, and its positive effects on society in the context of efficiency are immeasurable and emerging in our daily lives. According to an analysis by PwC, by 2030, AI could add £232BN to the Gross Domestic Product of the United Kingdom, which is approximately 10% higher than the current level. In the past few years, AI has become a key tool in space activities and the exploration of the universe, and it can be utilized for space communications, navigation, big data analysis, autonomy evaluation, decision support for spacecraft system design [3], space mission operations [4], [5], planetary defense, mapping the moon [6], space exploration [7] and universe exploration [8], among other tasks. Most previous works focused on space structure design, communications or flight simulations, and few have addressed the 'space tether'.

The original space tether concept came from the 'space elevator', which was proposed by a Russian scientist in 1895. A space tether is a type of lengthy cable ranging from a few hundred meters to many kilometers. The cable makes use of a few bundles of thin strands of high-strength fiber to couple spacecraft to every different or other masses, and it provides a mechanical connection that allows the transfer of energy and momentum from one object to the other. Space tethers can be utilised in many applications, collectively with studies of plasma physics and electrical science in the Earth's upper atmosphere, the orbiting or deorbiting of space vehicles, payload transfer, inter-planetary propulsion, and specialised missions, such as asteroid engagement or, in severe form, as a well-publicized space elevator [1]. With the

The associate editor coordinating the review of this manuscript and approving it for publication was Zhonglai Wang.

development of space technology, space tethers are broadly used in the exploration of Mars, or even deep space missions [2]. Recently, a few companies, e.g., Google and SpaceX, have been working on space projects related to space elevators, and these projects are mainly supported by developed AI tools.

To fill the current research gap, this paper utilizes an AI-driven design tool for payload orbital transfer via a space tether using a computational intelligence-assisted design (CIAD) framework [9], [10], [22], [28]. An intelligent design system is created with the artificial wolf pack algorithm (AWPA) [24], and this gadget presents three practical advantages: (1)the mobilisation and flexibility of computing resources; (2) the embedment of a set of AI algorithms, and (3) the reducing computational cost as a design objective. In this research, a symmetrical motorized momentum space tether (MMET) with a payload at each end experiences centripetal acceleration when rotating about a facility [1], [11], [12].

In the last a few decades, the studies on the nature-inspired AI algorithms have been widely performed, such as the family of genetic algorithms (GAs) [25], which were inspired by the Darwinian theory and the concept of survival of the fittest; swarm intelligence and algorithms, including the ant colony optimization in 1992, the particle swarm optimization (PSO) in 1995, the Artificial bee colony in 1996, and the firefly swarm algorithm (Firefly) in 2013 [27], and others, based on the principles of natural phenomena, which reproduce the social intelligence of the behaviour of an animal or insect swarm. As one of the most broadly used evolutionary algorithms, the GAs provide a near-optimal solution for practical problems with massive numbers of variables and constraints, in which, the best possible control parameters, including the size of population, the crossover operation rate and the mutation operation rate, are difficult to determine. The typical motivation behind developing nature-based algorithms is to effectively and efficiently solve different optimization problems. During Earth's natural development, it is assumed that the behavior of nature is usually optimal. In this research, the AWPA, a newly proposed nature-inspired algorithm, is utilised to achieve global solutions for space tether's continuous nonlinear functions in a space mission, with low computational effort and excessive consistency.

The remaining sections of this work are organized as follows. Section II introduces the social dynamic behaviors of a WP in the natural world, then it gives the AWPA algorithm with logsig randomness, which was stimulated by using the WP's swarm intelligence of its social behaviors, as added in Section II. To investigate the optimization performance, Section III defines the fashion indices for evolutionary optimization, which includes three pairs of trend indices. Section V offers the modeling of payload transfer the use of a house tether. Section VI discusses multi-objective optimization and fitness functions based on the relevant criteria. Section VII presents the empirical outcomes and a discussion of these results. Section VIII concludes this paper and gives potential details of future work.

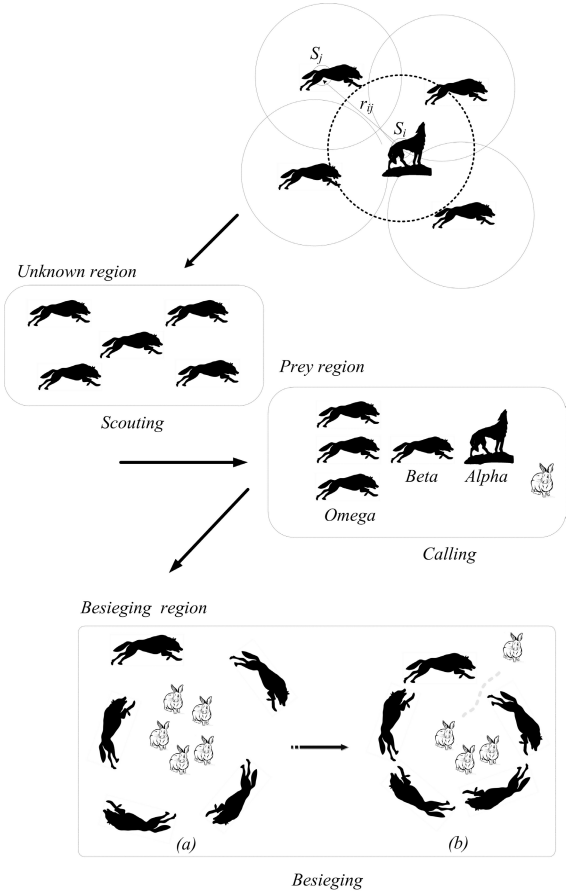

FIGURE 1. A WP's social behaviors.

II. WOLF PACK'S SOCIAL MECHANISM AND ARTIFICIAL WOLF PACK ALGORITHM

Wolves are gregarious animals who mostly live in packs. A wolf pack (WP) is formed when a male (α) and a female wolf (β) meet and continue to be together as a mated pair. The pair establishes a territory to settle and increase cubs in most years. The cubs stay within the WP until they are old enough to leave home, generally when they are 3 years old, and they can then start a WP of their own. Thus, the social structure of a WP consists of a permanent core of a $\alpha + \beta$ pair plus their continuously dispersing offspring. A WP has a very strict stage of hierarchy that need to be adhered to by all the members of the pack, and it supports the WP to survive. For their social intelligence, wolves are considered one of the smartest animals in nature, and they have developed the potential to live on in a vast vary of surroundings, which varies from the wilderness to humid swamps to the Arctic region with temperatures of $-40^{o}C$ and bitter winds.

Basically, a WP has 3 types of behaviors in their social activities, namely, 'scouting', 'calling' and 'besieging', as shown in Figure 1, usually in a WP, an α male wolf is the leader wolf who is in the decision-making position

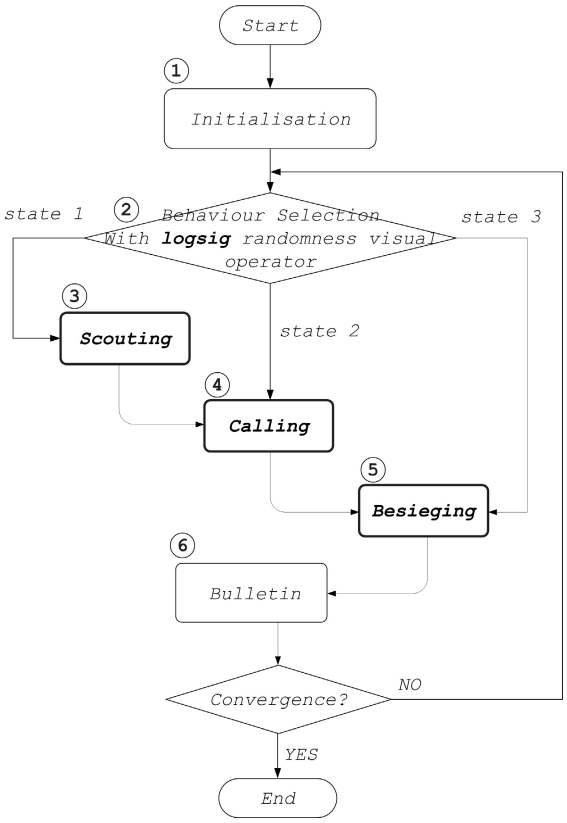

FIGURE 2. The workflow of artificial wolf pack algorithm.

```
Begin (1)

  t = 0 ;
  Initialise all parameters:
     x_i with variable population P,  fitness(x_0),
visual, try_number etc.

    While ( Not termination-condition) do
      Begin (2)

         t    =  t + 1;

        FOR i = 1: Population

            state = Behaviour Selection()
                IF( state ==1)
                   Scouting();

                Elseif (state ==2)
                   Calling();

                Elseif (state ==3)
                   Besieging();

                Else

                End

         ENDi

       evaluation fitness(x) and best solutions

      End (2)

End (1)
```

FIGURE 3. AWPA pseudo code.

and is able to command all the other wolves to carry out suitable actions. Specifically, *scouting*: the scout group of wolves are deployed to explore unknown areas; *calling*: when the scout wolves have spotted and positioned the prey in an area, they will report this information to the α wolf and also communicate with other wolves by their howling; *besieging*: after the α wolf confirms the prey information and will be leading the WP toward the scout wolves, starting the grey hunting and capturing actions in the so-called the besieging area.

Inspired by the swarm intelligence of a WP's social behaviors, an artificial intelligent algorithm, the Artificial Wolf Pack Algorithm (AWPA) is proposed by implementing three social behaviors of a WP, in which, there are six steps include: (1) initialization of all the variables; (2) the behavior selection from three social behaviors with the *logsig()* randomness; (3) the operation of *scouting* behavior; (4) the operation of *calling* behavior; (5) the operation of *besieging* behavior and (6) the bulletin step to summarise the results.

Without loss of generality, in this section, $S(*)j$ is considered the status of any $(*)$ artificial wolf with status j. The AWPA workflow is given in Figure 2. As shown in Equation (1), when performing the AWPA with a pre-defined function $WP_{M\times N}$, it first simulates the behavior of an individual artificial wolf (AW, as S_{ij}), where M is the population and N is the number of individuals in a WP. Each AW searches for the local optimal solution and passes its result to the self-organized WP and so as to obtain the optimal global solution.

As also shown in Figure 3, it gives the pseudocode implementation of the AWPA algorithm, in which, the 'max-generation' parameter is set as the terminal condition of the AWPA optimisation.

(1) Initialization: in this step, all the variables and parameters are set to the pre-defined values, in a case, population = 50, max generation = 200, etc., and the simulation program prepare for the subsequent steps.

$$WP_{M\times N} = \begin{bmatrix} S_{11} & S_{12} & \dots & S_{1q} & S_{1N} \\ S_{21} & S_{22} & \dots & S_{2q} & S_{2N} \\ & & \dots & & \\ S_{p1} & S_{p2} & \dots & S_{pq} & S_{pN} \\ & & \dots & & \\ S_{M1} & S_{M2} & \dots & S_{Mq} & S_{MN} \end{bmatrix} \quad (1)$$

(2) Behavior Selection: In the 'behavior selection', there are three types of 'states' to indicate three different types of behaviors of a WP, that is, 'scouting', 'calling' and 'besieging', in which, the 'scouting' state is set as the default state or initial behavior of each WP.

Depending on the companion's number and the visual conditions, the prey density in the hunting region can be defined in Equation (2).

$$visual(t) = logsig\left(\frac{\frac{T}{2} - t}{k}\right) \times random(t) \quad (2)$$

in which,

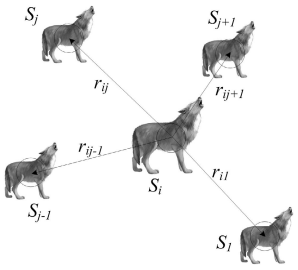

FIGURE 4. The Euclidean distance between the AWi^{th} and AWj^{th} and states updating.

- *logsig*() is a logarithmic sigmoid transfer function;
- T is the maximum number of iterations;
- t is the current iteration number;
- k changes the slope of the *logsig*() function;
- *random*() is a random value within the range of (0,1).

(3) Scouting: For an AW individual k in a WP, let's define S as the finite state set, and there are states 1 to M that an AW can perform, as given in Equation (3).

$$S_{(*)k} = \{s_1, \ldots, s_M\} \tag{3}$$

Within the AW's visual field, let's define $S_{(*)i}$ as the current state of an AW and $S_{(*)j}$ as the next state. Specifically, an AW moves from its current state $S_{(*)i}$ to the next state $S_{(*)j}$ randomly, and keep checking the state updating conditions, as stated in Equations (5) and (4), where ϵ is a random movement factor, δ is the iteration step, and υ is the visual constant of the AW. For a given AW, the prey density is defined as $F = f(S)$, in which, F is the fitness function, F_i and F_j are the prey density in the state $S_{(*)i}$ and $S_{(*)j}$, respectively.

$$S_{(*)j} = S_{(*)i} + \epsilon \cdot \upsilon \tag{4}$$

$$S_{(*)i+1} = \begin{cases} S_{(*)i} + \epsilon \cdot \delta, & if\, F_i \geq F_j \\ S_{(*)i} + \epsilon \cdot \delta \cdot \dfrac{S_{(*)j} - S_{(*)i}}{\|S_{(*)j} - S_{(*)i}\|}, & otherwise \end{cases} \tag{5}$$

As defined in Equation (6), r_{ij} is the Euclidean distance between the AWi^{th} and AWj^{th},also illustrated in Figure 4.

$$r_{ij} = \|S_{(*)j} - S_{(*)i}\| \tag{6}$$

(4) Calling: Let's set $S_{(*)c}$ as the the central state, η as the crowd factor, γ as the AW's neighbor number and F_c as the prey density of the central state, as given in Equation (7).

$$F_c = f(S_{(*)c}) \tag{7}$$

As given in Equation (8), when under the condition $C1$ as given in Equation (9): the AW performs the central state-driven 'Calling' behavior; Otherwise, the AW continues with 'Scouting' behavior, as defined in Equation (8), within the AW's visual field ($r_{ij} < \upsilon$).

$$S_{(*)i+1} = \begin{cases} S_{(*)i} + \dfrac{S_{(*)c} - S_{(*)i}}{\|S_{(*)c} - S_{(*)i}\|} \cdot \epsilon \cdot \delta & \text{if } C1 \\ (5) & otherwise \end{cases} \tag{8}$$

$$C1 == \left(\frac{F_c}{\gamma} > \eta F_i\right) \&\& (\eta \geq 1) \tag{9}$$

(5) Besieging:

When a WP in its S_{max} states, that is, it is reaching to the "max" state, let's define F_{max} as the max or highest prey density, and there are γ individuals in the neighborhood.

As shown in Equation (10), when under the condition $C2$ as given in Equation (11): the AW performs the central state-driven 'Besieging' behavior, that is, the AW keeps updating the state in the F_{max} region; Otherwise, the AW continues with 'Scouting' behavior, as defined in Equation (8).

$$S_{(*)i+1} = \begin{cases} S_{(*)i} + \dfrac{S_{max} - S_{(*)i}}{\|S_{max} - S_{(*)i}\|} \cdot \epsilon \cdot \delta & \text{if } C2 \\ (5) & otherwise \end{cases} \tag{10}$$

$$C2 == \left(\frac{F_{max}}{\gamma} > \eta F_i\right) \&\& (\eta \geq 1) \tag{11}$$

(6) Bulletin: The bulletin step compares the current state $S_{(*)i}$ of each AW with the historical state data. The bulletin data are replaced and updated only when the current state is better than the previous state, as described by Equation (12).

In the bulletin step, there is a data pool, to contain the 'bulletin data'. This step compares the current state $S_{(*)i}$ of all the AW population with their historical data. As given in Equation (12): the bulletin data are replaced and updated only when the current state is better than the previous state; Otherwise, the bulletin data keep as they are. Then the bulletin data are moving to the next loop.

$$S_{(*)j+1} = \begin{cases} S_{(*)i} & \text{if } F_i \geq F_j \\ S_{(*)j} & \text{otherwise} \end{cases} \tag{12}$$

III. THREE PAIRS OF TREND INDICES

To evaluate the performance of the optimization process, and benchmarks for the AWPA algorithm, three pairs of trend indices are introduced in this section:

1) the trend index of moving mean of the average precision (*mmAP*) and the index of moving mean of the standard deviation (*mmSTD*), as given in equations (13) and (14), respectively;
The trend index of *mmAP* is defined as a moving average score of the *MEAN* value of a vector f_j, as given in equation (13), in which $i = 1, 2, \cdots, j, \cdots, p$, p is the size of the dataset's population, $MEAN(\cdot)$ is the average function.
The trend index of *mmSTD* is a moving average score of the *STD* value of vector f_j, as given in equation (14), in which $STD(\cdot)$ is the standard deviation function.

$$mmAP\left(f_j\right) = MEAN \sum_{i=1}^{p} \left(\frac{1}{i} \sum_{j=1}^{i} MEAN\left(f_j\right)\right) \tag{13}$$

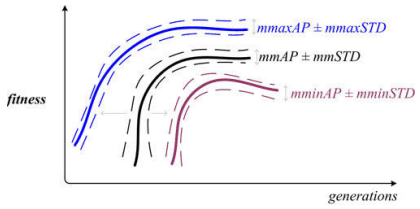

FIGURE 5. The definition of evolutionary pathway.

$$mmSTD\left(f_j\right) = MEAN\sum_{i=1}^{p}\left(\frac{1}{i}\sum_{j=1}^{i}STD\left(f_j\right)\right) \tag{14}$$

Both indices of *mmAP* and *mmSTD* are employed to assess the short-term fluctuations by recording the long-term trend throughout their evolutionary process.

2) the trend index of 'moving max of the average precision' (*mmaxAP*) and the index of 'moving max of the standard deviation' (*mmaxSTD*), as given in equations (15) and (16), respectively.

$$mmaxAP\left(f_j\right) = MAX\sum_{i=1}^{p}\left(\frac{1}{i}\sum_{j=1}^{i}MAX\left(f_j\right)\right) \tag{15}$$

$$mmaxSTD\left(f_j\right) = MAX\sum_{i=1}^{p}\left(\frac{1}{i}\sum_{j=1}^{i}STD\left(f_j\right)\right) \tag{16}$$

3) the trend index of moving min of the average precision (*mminAP*) and the index of moving min of the standard deviation (*mminSTD*),as given in equations (17) and (18), respectively.

$$mminAP\left(f_j\right) = MIN\sum_{i=1}^{p}\left(\frac{1}{i}\sum_{j=1}^{i}MIN\left(f_j\right)\right) \tag{17}$$

$$mminSTD\left(f_j\right) = MIN\sum_{i=1}^{p}\left(\frac{1}{i}\sum_{j=1}^{i}STD\left(f_j\right)\right) \tag{18}$$

IV. EVOLUTIONARY PATHWAY

As shown in Figure 5, from top to bottom, the **solid** lines are the trend indices of *mmaxAP*, *mmAP* and *mminAP* of a fitness function in a vector f_j, as given in equations (15), (13) and (17), respectively.

The **dashed** lines are the boundaries of *mmaxAP* ± *mmaxSTD*, *mmAP* ± *mmSTD* and *mminAP* ± *mminSTD* values for each vector f_j, as defined in Equations (16), (14) and (18), which illustrate the tracking shape of the *evolutionary pathway* for the optimization process, *generation* versus *fitness f* in this case, as the upper and lower boundaries.

V. PAYLOAD TRANSFER USING SPACE TETHER UNDER UNCERTAINTIES

As illustrated in Figure 6, there are two sub-figures labelled as (a) and (b), which describes the orbital elements of payload release and transfer using space tether.

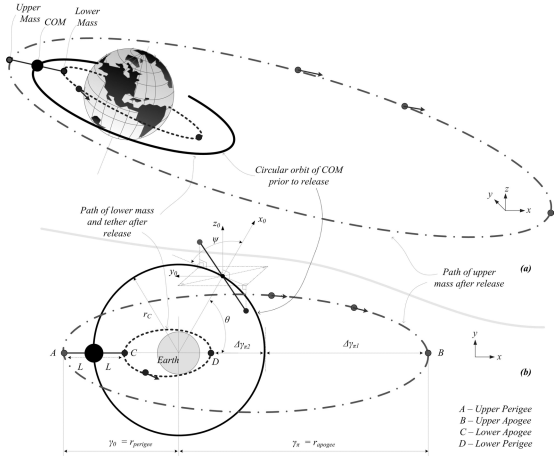

FIGURE 6. Orbital elements of payload release and transfer.

- Figure 6 (a), it demonstrates the payload transfer from a 3D perspective.
- Figure 6 (b), it describes the parameters for modeling of the payload transfer from a 2D perspective.

Generally, the space tether's payload transfer is in a low Earth orbit, where the space tether obtains rising angular velocity than it requires to remain in the orbit, however, it does not comprise sufficient energy to escape from the Earth's gravity field.

During payload transferring, a robotic space tether, consists of a few modules including: the upper payload, the lower payload and a center of mass (COM), is in a low Earth orbit, where the upper payload can be released from the spinning space tether with enough angular momentum, which is aligned along the local gravity vector.

After the release operation, the upper payload will enter an elliptical orbit (named as 'OU'), as shown in both sub-figures (a) and (b), in which the **point A** (the upper perigee of 'OU') is the release point. Then, half of moving on the elliptical orbit later, the upper payload reaches the **point B** (the upper apogee of 'OU'), where is further from the Earth than it was at release point.

On the contrary, the lower payload will not have enough energy to maintain in its circular orbit after the release operation, and it will enter into another elliptical orbit (named as 'LU'). Upon reaching the **point D** (the perigee of 'LU'), the lower payload is closer to the Earth than it was at the release **point C** (the apogee of 'LU').

Finishing above actions, the upper and lower masses of payloads are released from the spinning space tether, entering a raised orbit and lowered orbit, respectively.

All the environmental effects that can influence the space tether modelling are assumed to be negligible in the space tether's modelling context, including solar radiation, aerodynamic drag, electrodynamic forces and no frictional losses.

To build a model for the payload transfer, a set of parameters are defined here,

- Δr_{π_i}, 'tether performance index': the radial separation, which is the distance between the payload and the facility's orbit at the time of release, that is, the half an orbit after the tether releases the payload. As called as the 'tether performance index' [19], the value of Δr_{π_i} describes how well the space tether facility performs at transferring the payload.
  When $i = 1$, it defines the Δr_{π_i} of the upper payload, and when $i = 2$, it defines the Δr_{π_i} of the lower payload, as given in Equations(19) and (20),respectively.
- τ_1: the 'upper payload efficiency' index, which is the perigee altitude loss of the upper payload,as given in Equation (21). For the upper payload, when it is released at **point A**, and a larger apogee altitude gain of τ_1 indicates excellent tether transfer performance.
- τ_2: the 'lower payload efficiency' index, the perigee altitude loss of the lower payload,as given in Equation (22). For the lower payload, when it is released at **point C**, a smaller perigee altitude loss of τ_2 reflects better tether transfer performance. The 'tether efficiency indices' τ_1 and τ_2 are introduced to to assess the efficiency of payload transfer.
- r_c: the radius of circular orbit of the COM prior to release.
- L: the length of the tether sub-span.
- l: the length of tether, where $l \in [0, L]$.
- $\dot{\psi}$: the angular pitch velocity.
- $\dot{\theta}$: the angular orbital velocity.
- μ: the standard gravity of Earth, which is $3.9877848\times10^{14}\ m^3s^{-2}$.
- σ: the tensile stress in the tether, generated by the rotation of the space tether system with the assumption that the gravity gradient effects are negligible, as defined by Equation (25).
- σ_0: the maximal tether stress.
- σ_{LIM}: the safe stress limit of the tether sub-span. As shown in Equation (26), the maximal tether stress must stay within the safe stress limit of the tether, that is $\sigma_0 \leq \sigma_{LIM}$.
  Equations (25) and (26) describe the symmetrical stress distribution within symmetrical space tether's sub-spans [19], [20], where the payloads connect to the tether and the maximal stress of the full tether sub-span is given by equation (26).

$$\Delta r_{\pi_1} = \frac{(r_c+L)^2\left[(r_c+L)\,\dot{\theta}+L\dot{\psi}\right]^2}{2\mu-(r_c+L)\left[(r_c+L)\,\dot{\theta}+L\dot{\psi}\right]^2} - r_c \quad (19)$$

$$\Delta r_{\pi_2} = \frac{(r_c-L)^2\left[(r_c-L)\,\dot{\theta}-L\dot{\psi}\right]^2}{2\mu-(r_c-L)\left[(r_c-L)\,\dot{\theta}-L\dot{\psi}\right]^2} - r_c \quad (20)$$

$$\tau_1 = \frac{\Delta r_{\pi_1}}{L} \quad (21)$$

$$\tau_2 = \frac{\Delta r_{\pi_2}}{L} \quad (22)$$

To perform the simplification for the Equations (21) and (22) by fulfilling a binomial expansion, let's involve an additional assumption of $L \ll r_c$, and cause to the result of $\frac{L}{r_c} \ll 1$, which can be employed to obtain the reformations as (23) and (24).

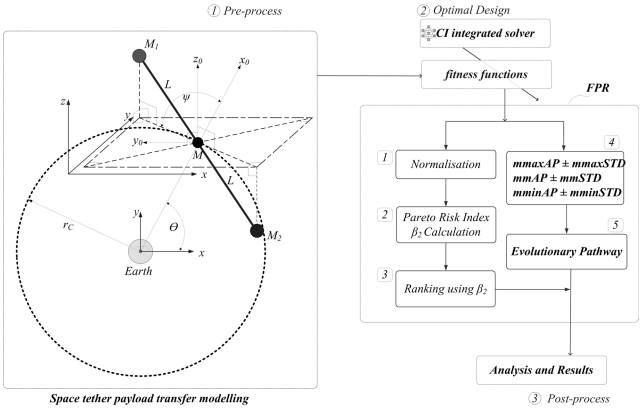

FIGURE 7. Optimisation of space tether for payload orbital transfer via CIAD framework.

$$\tau_1 = 7 + \frac{30L}{r_c} + \frac{4\dot{\psi}}{\dot{\theta}} + \frac{2Lr_c^2\dot{\psi}\left(18\dot{\theta}+5\dot{\psi}\right)}{\mu} \quad (23)$$

$$\tau_2 = -7 + \frac{30L}{r_c} - \frac{4\dot{\psi}}{\dot{\theta}} + \frac{2Lr_c^2\dot{\psi}\left(18\dot{\theta}+5\dot{\psi}\right)}{\mu} \quad (24)$$

$$\sigma = \frac{1}{A}\dot{\psi}^2 l\left(M_P + \frac{1}{2}\rho A l\right) \quad (25)$$

$$\sigma_0 = \sigma|_{l=L} = \frac{1}{A}\dot{\psi}^2 L\left(M_P + \frac{1}{2}\rho A L\right) < \sigma_{LIM} \quad (26)$$

VI. FITNESS FUNCTIONS AND OPTIMAL DESIGN CRITERIA

As shown in Figure 7, the multi-objective optimization process of the space tether for payload orbital transfer includes four steps, as listed below.

1) Pre-processing: This step includes the dynamic modeling of the space tether for payload orbital transfer, as given in Section V;
2) The optimal design given by the computational intelligence approaches via the integrated solver;
3) Three design objectives. The MMET payload transfer and design strength problems are defined as three conflicting objectives that need to be balanced in the optimization study, in which the practical multi-objective problem of tether payload transfer can be expressed as follows [20].
   a) Upper payload transfer, as given in Equation (27).

$$Maximise: f_1\left(\dot{\psi}, L\right) = \tau_1 \quad (27)$$

   b) Lower payload transfer, where, ε is a parameter with a small value that helps avoid $f_2 \longrightarrow \infty$ and $\varepsilon \longrightarrow 0$, as given in Equation (28).

$$Maximise: f_2\left(\dot{\psi}, L\right) = \frac{1}{\tau_2 + \varepsilon} \quad (28)$$

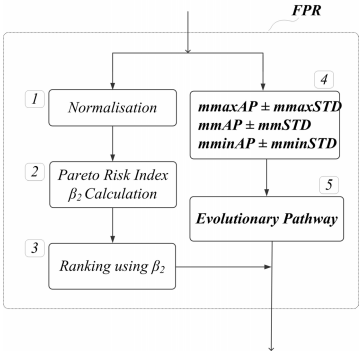

FIGURE 8. The FPR flowchart.

c) Tether strength, as given in Equation (29).

$$Maximise: f_3\left(\dot{\psi}, L, A\right) = \sigma_{LIM} - \sigma_0 \quad (29)$$

4) Fitness function with the FPR approach;
As shown in Equation (30), a multi-objective optimization problem are stated, in which,

- F_i, the fitness functions, where $\Re^n \to \Re$.
- x, decision variable vector.
- J, the number of F_i.
- M, the number of the equality constraints.
- I, the number of the inequality constraints.
- K, the number of variables

$$\begin{aligned} Maximise: F_i(x) &= [f_1(x), f_2(x), \cdots, f_J(x)] \\ x &= [x_1, x_2, \cdots, x_K] \\ i &= 1, 2, \cdots, J \end{aligned} \quad (30)$$

a) *Fast approach for Pareto-optimal solution recommendation*
Thus, based on the three design objectives given in Equations (27), (28) and (29), in this section, the three pairs of trend indices are used to establish a fast approach for Pareto-optimal solution recommendation (FPR) [21], [23], to define a fitness function, to investigate the multi-objective problem, and to build the evolutionary pathway for the optimization process.
As shown in Figure 8, the FPR using a Pareto risk index (β_2) can be outlined in five sub-steps, which include (1) normalization, (2) calculating the Pareto risk index β_2, (3) ranking using β_2, (4) calculating the three pairs of trend indices, and (5) generating the evolutionary pathway, as discussed in Section III.

b) *Normalization process*
The normalization process involves the mapping of the variables from their original value range to a normalized value range [1], e.g., [0, 1], by two operations *scale* and *shift*. As defined in Equation (30), the vector of objective functions F_i is the raw data source of the normalization block, in which $f_i \in [f_{min}, f_{max}]$. $\|F_i\|$ is the normalized values of F_i.

c) *Pareto Risk Index*
The Pareto Risk Index (β_2) is defined by Equation (31),

$$\beta_2(f_i) = \frac{\sigma_f}{\mu_f} \quad (31)$$

where,

- μ_f, the mean value of the normalized objectives, as defined in Equation (32).

$$\mu_f = \frac{\sum_i^J W_i}{J} \quad (32)$$

- σ_f, the standard deviation of the normalized objectives, as defined in Equation (33).

$$\sigma_f^2 = \frac{\sum_i^J \left(W_i - \mu_f\right)^2}{J-1} \quad (33)$$

- W_i, the weighted normalized objective, as given in Equation (34).

$$W_i = w_i \cdot f_{i_h} \quad (34)$$

- w_i, the weight factor, which balances the weights of the normalized objectives, under the conditions: $w_i \in [0,1]$ and $\sum_i^J w_i = 1$.

d) *Fitness Function Definition*
The FPR provides users with a recommended list of optimal ranking and optimal trend indications with different risk tolerance values and is used to determine the optimal trade-offs between the three conflicting design objectives for the payload transfer mission involving a space tether, as discussed above.

$$Maximise: F = mmaxAP\{\|\beta_2(f_1, f_2, f_3)\|\} \quad (35)$$

5) Post-processing: This step involves analyzing and visualizing the optimal results and presenting the outputs.

VII. OPTIMAL DESIGN FOR ORBITAL PAYLOAD TRANSFER

The computers used for the simulations have Intel Core i7-5500U 2.4 GHz dual-core processors with the Windows 7 flagship x64 service pack 1, 8.0-GB 1600-MHz dual-channel DDR3L SDRAM, and MATLAB R2010a.

Table 1 lists the parameters for the optimization process, in which, the termination condition is set to' max-generation = 100' for each loop of evolutionary optimisation; the try variable is 5; the population is 50; the total number of tests is 100; the iteration step is 0.001; the initial visual value is 2.5; the crowd value is 0.618.

Table 2 gives the optimal combinations (MEAN±STD) of F and the design variables (x_1, x_2, x_3), and the results indicate that the overall performance of the AWPA in the optimal

TABLE 1. Parameters for orbital payload transfer.

	max-generation	200
	population	50
	test-number	100
	try-number	5
	iterate step	0.001
	initial visual	2.5
	crowd	0.618
σ_{LIM}	stress limit	5 GPa
ρ	tether density	970 kgm^{-3}
r_c	circular orbit radius of space tether's COM at payload release	6890 m
μ	gravitational constant	3.9877848×10^{14} m^3s^{-2}
e	eccentricity	0
x_1	ψ	$[1\times10^{-5}, 1]$ rad/s
x_2	L	$[1\times10^{3}, 2.5\times10^{5}]$ m
x_3	A	$[5\times10^{-6}, 5\times10^{-1}]$ m^2

TABLE 2. Optimal results of payload transfer.

	F		x_1	x_2		x_3	
AWPA	**0.9968**	±	0.1821±	1.634e5	±	0.3841	±
	3.2e-5		0.0576	1.472e2		0.02231	
Firefly	0.9784	±	0.2354±	2.012e5	±	0.5643	±
	7.1e-5		0.0433	2.633e2		0.1065	
GA	0.9769	±	0.2165±	1.834e5	±	0.6424	±
	4.2e-5		0.0186	1.644e2		0.06587	

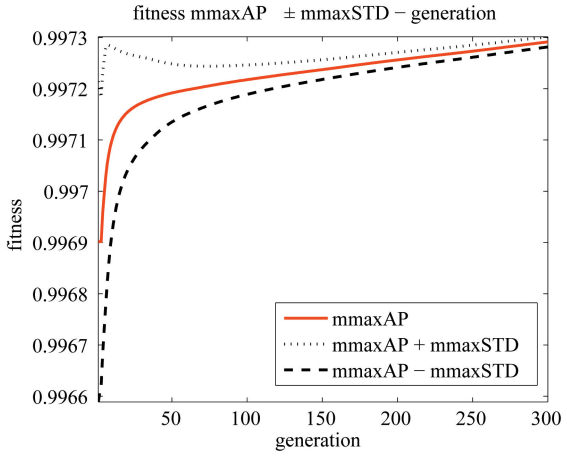

FIGURE 9. Optimal design process: *mmaxAP* ± *mmaxSTD*.

design of a space tether for orbital payload transfer is better than that of the firefly algorithm and GA.

Figures 9 to 12 give the *max*, *mean* and *min* fitness curves, which show that the AWPA converge near generation 30.

Figure 9, Figure 10 and Figure 11 show the *mmaxAP* ± *mmaxSTD*, *mmAP* ± *mmSTD* and *mminAP* ± *mminSTD* fitness curves over the full simulation period, respectively.

Figure 12 illustrates the evolutionary pathway of the optimization process of the optimal design for space tether payload transfer using the *mmaxAP* ± *mmaxSTD*, *mmAP* ± *mmSTD* and *mminAP* ± *mminSTD* fitness curves with their upper and lower boundaries.

Obviously, the fitness values increases very quickly, and it reaches a plateau from generations 1 to 250. All curves converge from generation 280 to 300, which reflects the high efficiency of the proposed AWPA for this space tether payload transfer application.

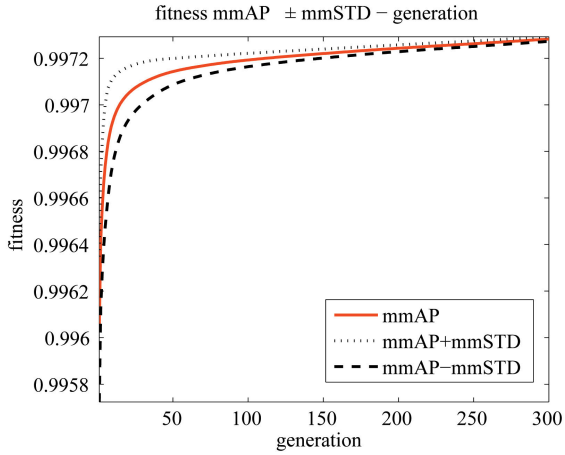

FIGURE 10. Optimal design process: *mmAP* ± *mmSTD*.

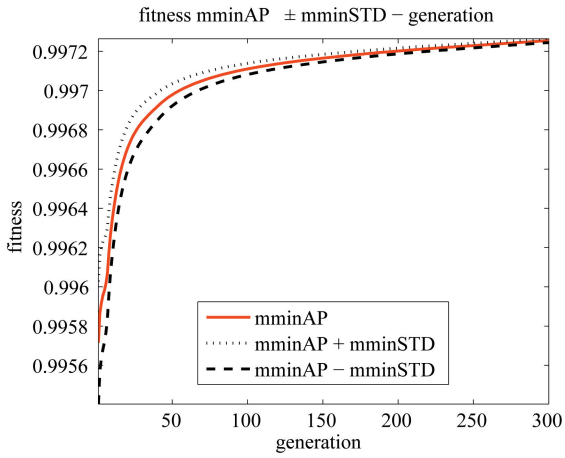

FIGURE 11. Optimal design process: mminAP ± *mmSTD*.

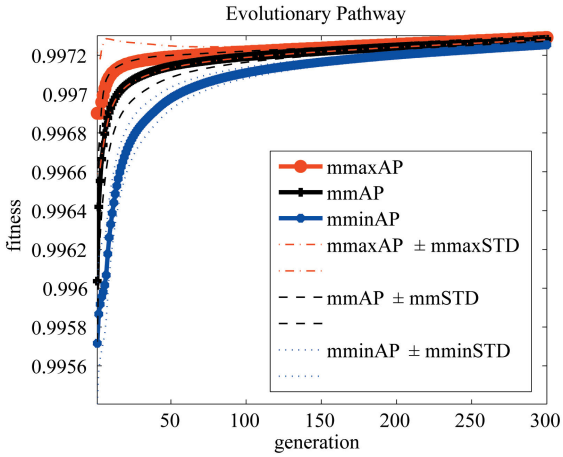

FIGURE 12. Evolutionary pathway of space tether payload transfer.

VIII. CONCLUSIONS AND FUTURE WORKS

In this study, the efficiency of payload transfer τ_1 considering the perigee altitude loss τ_2 and tether stress σ are defined for space tether payload orbital transfer, and three fitness functions are obtained using the newly devised trend indices for

the multi-objective problem. Then, optimization is performed with the newly developed multi-objective AWPA.

The following conclusions can be drawn with the results and discussions above:

- The optimal design using the multi-objective AWPA exhibits good agreement with previous results.
- The evolutionary trends are accurately reflected by the three defined pairs of trend indices with variable uncertainty and tolerance levels.

The contributions of this research are as follows:

- the dynamic evolutionary behaviors of three pairs of trend indices are obtained and considered in optimization.
- the fast Pareto-optimal solution recommendation method is introduced, and a clear recommendation list is established for decision making.
- β_2 is used to rank the uncertainties of the Pareto-optimal solutions.
- a multi-objective AWPA is developed.

The future research will focus on the following aspects:

- further studies on the implementation of experimental verification and validation for the space tether and space robotic and autonomous system;
- the development of the operational strategy of high efficient payload transfer using space tether systems;
- the studies on the high efficiency and reliability design for the key components of the space tethers;
- to develop a computational intelligence assisted design software package for industrial design and manufacture, as one of the components of cyber-physical system (CPS) for industry 4.0 applications in future space projects, using cutting-edge technologies, such as: 'digital twin' and internet of things;
- more studies on new AI algorithms, such as heredity algorithm and swarm dolphin algorithm, will be applied to search for the recommended solutions of both an optimisation process and a decision process with the support of the parallel CIAD framework [10];
- more works on reliability-based design and optimisation via virtual and experiment-based model validation [13]–[18].

REFERENCES

[1] Y. Chen, "Dynamical modelling of a flexible motorised momentum exchange tether and hybrid fuzzy sliding mode control for spin-up," Ph.D. dissertation, Dept. Mech. Eng., Univ. Glasgow, Glasgow, Scotland, 2010.

[2] Y. Chen, R. Huang, X. Ren, L. He, and Y. He, "History of the tether concept and tether missions: A review," *ISRN Astron. Astrophys.*, vol. 2013, Feb. 2013, Art. no. 502973.

[3] D. Girimonte and D. Izzo, "Artificial intelligence for space applications," in *Intelligent Computing Everywhere*, A. J. Schuster, Eds. London, U.K.: Springer, 2007.

[4] S. Chien and R. Morris, "Space applications of artificial intelligence," *AI Mag.*, vol. 35, no. 4, pp. 3–6, Dec. 2014.

[5] ESA. *Increasing Use of Artificial Intelligence in Satellite Operations*. Accessed: Apr. 20, 2018. [Online]. Available: http://spaceref.com/nasa-hack-space/increasing-use-of-artificial-intelligence-in-satellite-operations.html

[6] K. Bourzac. *AI in Space*. Accessed: Apr. 20, 2018. [Online]. Available: https://spectrum.ieee.org/tech-talk/robotics/artificial-intelligence/ai-in-space

[7] T. Maciel. (2017). *Artificial Intelligence in Space-Three Reasons Why Artificial Intelligence is Key to Space Exploration*. Accessed: Apr. 20, 2018. [Online]. Available: https://spacecentre.co.uk/blog-post/artificial-intelligence-space/

[8] J. Vincent. *AI Could be the Perfect Tool for Exploring the Universe*. Accessed: Apr. 20, 2018. [Online]. Available: https://www.theverge.com/2017/11/15/16654352/ai-astronomy-space-exploration-data

[9] Y. Chen, Z. Song, G. Zhang, M. T. Majeed, and Y. Li, "Spatio-temporal evolutionary analysis of the township enterprises of Beijing suburbs using computational intelligence assisted design framework," *Palgrave Commun.*, vol. 4, Mar. 2018, Art. no. 31.

[10] Y. Chen and Y. Li, *Computational Intelligence Assisted Design: In Industrial Revolution 4.0*. Boca Raton, FL, USA: CRC Press, 2018.

[11] M. P. Cartmell and D. J. McKenzie, "A review of space tether research," *Prog. Aerosp. Sci.*, vol. 44, no. 1, pp. 1–21, 2008.

[12] Y. Chen, R. Huang, L. He, X. Ren, and B. Zheng, "Dynamical modelling and control of space tethers: A review of space tether research," *Nonlinear Dyn.*, vol. 77, no. 4, pp. 1077–1099, 2014, doi: 10.1007/s11071-014-1390-5.

[13] Z. Wang, X. Cheng, and J. Liu, "Time-dependent concurrent reliability-based design optimization integrating experiment-based model validation," *Struct. Multidisciplinary Optim.*, vol. 57, no. 4, pp. 1523–1531, 2018.

[14] S. Yu, Z. Wang, and K. Zhang, "Sequential time-dependent reliability analysis for the lower extremity exoskeleton under uncertainty," *Rel. Eng. Syst. Saf.*, vol. 170, pp. 45–52, Feb. 2018.

[15] S. Yu and Z. Wang, "A novel time-variant reliability analysis method based on failure processes decomposition for dynamic uncertain structures," *ASME J. Mech. Des.*, vol. 140, no. 5, 2018, Art. no. 051401.

[16] S. Yu, Z. Wang, and D. Meng, "Time-variant reliability assessment for multiple failure modes and temporal parameters," *Struct. Multidisciplinary Optim.*, vol. 58, no. 4, pp. 1705–1717, 2018.

[17] Z. Wang, S. Yu, L. Y. Chen, and Y. Li, "Robust design for the lower extremity exoskeleton under a stochastic Terrain by mimicking wolf pack behaviors," *IEEE Access*, vol. 6, pp. 30714–30725, 2018.

[18] Z. Wang, Z. Wang, S. Yu, and K. Zhang, "Time-dependent mechanism reliability analysis based on envelope function and vine-copula function," *Mechanism Mach. Theory*, vol. 134, pp. 667–684, Apr. 2019.

[19] S. W. Ziegler and M. P. Cartmell, "Using motorized tethers for payload orbital transfer," *J. Spacecraft Rockets*, vol. 38, no. 6, pp. 904–913, 2001.

[20] Y. Chen and M. P. Cartmell, "Multi-objective optimisation on motorised momentum exchange tether for payload orbital transfer," in *Proc. IEEE Congr. Evol. Comput. (CEC)*, Singapore. Piscataway, NJ, USA: IEEE Computer Society, Sep. 2007, pp. 987–993.

[21] Y. Chen, B. Peng, X. Hao, and G. Xie, "Fast approach of Pareto-optimal solution recommendation to multi-objective optimal design of serpentine-channel heat sink," *Appl. Therm. Eng.*, vol. 70, no. 1, pp. 263–273, 2014.

[22] Y. Chen, G. Zhang, T. Jin, S. Wu, and B. Peng, "Quantitative modelling of electricity consumption using computational intelligence aided design," *J. Cleaner Prod.*, vol. 69, pp. 143–152, Apr. 2014.

[23] X. Ren and Y. Chen, "Optimal micro-motion unit decomposition-based reliability allocation for computer numerical control machine using the swarm bat algorithm," *IEEE Access*, vol. 7, pp. 83556–83568, 2019.

[24] Y. Chen. *SwarmWolf–The Artificial Wolf Pack Algorithm (AWPA)*. Accessed: Apr. 20, 2018. [Online]. Available: https://uk.mathworks.com/matlabcentral/fileexchange/48469

[25] Y. Chen. *Simple Genetic Algorithm Laboratory Toolbox for MATLAB*. Accessed: Jul. 13, 2019. [Online]. Available: http://www.mathworks.co.uk/matlabcentral/fileexchange/5882

[26] Y. Chen. *SECFLAB—Simple Econometrics and Computational Finance Laboratory Toolbox*. Accessed: Jul. 13, 2019. [Online]. Available: http://www.mathworks.com/matlabcentral/fileexchange/38120

[27] Y. Chen. *SwarmFireFly—The Firefly Swarm Algorithm (FFSA)*. Accessed: Jul. 13, 2019. [Online]. Available: https://www.mathworks.com/matlabcentral/fileexchange/38931

[28] Y. Chen and Y. Li, "Intelligent autonomous pollination for future farming—A micro air vehicle conceptual framework with artificial intelligence and human-in-the-loop," *IEEE Access*, vol. 7, pp. 119706–119717, 2019.

XIANLIN REN (M'11) received the B.Sc., M.Sc., and Ph.D. degrees in mechanical engineering from Chongqing University, in 1999, 2004, and 2010, respectively. He is currently an Assistant Professor of mechanical and electrical engineering with the University of Electronic Science and Technology of China and the Institute of Electronic and Information Engineering of UESTC in Guangdong, the Director of the Industrial Internet and Intelligent Manufacturing Institute, a member of the China Quality Association, a member of Sichuan Science and Technology Association, and a member of the National Association of Basic Research on Interchangeability and Measurement Technology. He has served as PI or Co-PI for over twenty research projects, including the National Natural Science Foundation Youth Foundation, the Natural Science Foundation General Projects, the Natural Science Foundation Key Projects, the National 863 Projects, the National Major Projects, and the Transverse Projects of Enterprises. He has published over 60 journal and conference papers, and has six authorized patents. His research interests mainly include intelligent manufacturing systems, quality engineering, reliability modeling, reliability-based design optimization, and model validation.

YI CHEN (M'10–SM'17) received the B.Sc., M.Sc., and Ph.D. degrees. He has been taking a leading role in previous and current department to maintain multidisciplinary research links, and develop external research collaborations both nationally and internationally. He has also been leading a few research grants in the areas of artificial intelligence, high-performance computing, robotics and autonomous systems, and also studies in multidiscipinary contexts. He has a high-level output of research publications in leading international journals and presentations at international conferences, which related to the research area of robotics, digital manufacturing, and industry 4.0, which demonstrates significant research and grant potential in engineering and cross-disciplinary applications. He has published over 100 academic articles in both high impact international academic journal and international conferences and has been selected as a Publons' top 1% of reviewers in computer science and engineering. He is a member of IET, AAAI, AIAA, and ASME, a Fellow of HEA, and a Fellow of IMechE. He is also a Chartered Engineer. He has been actively involved in both academic research and KTP projects as PI and CoI funded by EPSRC (U.K.), Horizon2020 (EU), NSFC (China), National Key Research and Development Program of China, and Industrial funding bodies. He is one of the co-organizers of the WCCI'16 Special Session on Computational Intelligence for Industry 4.0 and CEC'19 Special Session on Evolutionary Computation for Creativity, Manufacture and Engineering Management in the Industry 4.0 Era. Besides, he is an Editorial Board member, and he has been a Guest Editor for five special issues.